GEOPHYSICS, VOL. 82, NO. 5 (SEPTEMBER-OCTOBER 2017); P. Q39–Q51

Interferometric OBS imaging for wide-angle seismic data

Kazuya Shiraishi, Gou Fujie, Takeshi Sato, Susumu Abe, Eiichi Asakawa, and Shuichi Kodaira

ABSTRACT

Marine wide-angle seismic data obtained using air guns and ocean-bottom seismographs (OBSs) are effective for determining large-scale subseafloor seismic velocities, but they are ineffective for imaging details of shallow seismic reflection structures because of poor illumination. Surface-related multiple reflections offer the potential to enlarge the OBS data illumination area. We have developed a new seismic imaging method for OBS surveys applying seismic interferometry, a technique that uses surface-related multiples similarly to mirror imaging. Seismic interferometry can use higher order multiple reflections than mirror imaging, which mainly uses first-order multiple reflections. A salient advantage of interferometric OBS imaging over mirror imaging is that it requires only single-component data, whereas mirror imaging requires vertical geophone and hydrophone components to separate upgoing and downgoing wavefields. We applied interferometric OBS imaging to actual 175 km long wide-angle OBS data acquired in the Nankai Trough subduction zone. We obtained clear continuous reflection images in the deep and shallow parts including the seafloor from the OBS data acquired with large spacing. Deconvolution interferometry is more suitable than correlation interferometry to improve spatial resolution because of the effects of spectral division when applied to common receiver gathers. We examined the imaging result dependence on data acquisition and processing parameters considering the data quality and target depth. An air-gun-to-OBS distance of up to 50 km and a record length of 80 s were necessary for better imaging. In addition, our decimation tests confirmed that denser OBS spacing yielded better quality and higher resolution images. Understanding crosstalk effects due to the acquisition setting will be useful to optimize methods for eliminating them. Interferometric OBS imaging merged with conventional primary reflection imaging is a powerful method for revealing crustal structures.

INTRODUCTION

Most marine active source seismic surveys are divisible into two categories: the multichannel seismic (MCS) survey using dense receiver cables and the wide-angle reflection and refraction seismic survey using ocean-bottom seismographs (OBSs). The MCS surveys generally use dense shot and receiver spacing. One can expect higher spatial resolution from MCS surveys than that provided by OBS surveys. However, because the cable length limits the offset range, seismic velocities, especially for deeper regions, are not well-constrained by MCS data alone. In contrast, OBS surveys use a long offset distance, which supports the development of well-constrained seismic velocity models using traveltime or full-waveform inversion. Nevertheless, some difficulties exist for reflection imaging using OBS data. First, wide-angle reflections and refractions recorded in OBS surveys lack high-frequency components. Second, shallow reflectors, including seafloor topography, cannot be imaged continuously because of sparse OBS spacing.

To enlarge the imaging area, one must use surface-related multiple reflections observed at the OBS survey because the imaging area by primary reflections is extremely narrow. Mirror imaging (Grion et al., 2007; Dash et al., 2009; Hanafy et al., 2015), an effective

Manuscript received by the Editor 12 September 2016; revised manuscript received 14 April 2017; published ahead of production 18 May 2017; published online 27 June 2017.
[1]Japan Agency for Marine-Earth Science and Technology, Research and Development Center for Ocean Drilling Science, Yokohama, Japan. E-mail: kshiraishi@jamstec.go.jp.
[2]Japan Agency for Marine-Earth Science and Technology, Research and Development Center for Earthquake and Tsunami, Yokohama, Japan. E-mail: fujie@jamstec.go.jp; tsato@jamstec.go.jp; kodaira@jamstec.go.jp.
[3]Japan Petroleum Exploration Co., Ltd., Tokyo, Japan. E-mail: susumu.abe@japex.co.jp.
[4]JGI Inc., Tokyo, Japan. E-mail: eiichi.asakawa@jgi.co.jp.

model-based method to use those multiple reflections, requires wavefield separation into primary reflections (upgoing) and first-order multiple reflections (downgoing) by P-Z summation. Then, those reflection signals are migrated based on a mirrored velocity model (Grion et al., 2007). However, wavefield separation is not straightforward because high-quality consistent responses are necessary for vertical geophone and hydrophone sensors.

Another effective method is seismic interferometry for redatuming useful signals at the original source or receiver locations by crosscorrelating the seismic traces (Schuster, 2009; Wapenaar et al., 2010). This approach presents several advantages over mirror imaging. As a data-driven redatuming technique, no velocity information is required for redatuming. Theoretically, not only first-order multiples but also higher order multiples are available. Furthermore, this method requires only a single component: just a vertical component of a geophone or a hydrophone component. This simple requirement represents a considerable advantage over mirror imaging when wavefield separation is not possible because of limitations of instruments and data quality. For example, differences in the dynamic range and impulse responses between the vertical component and hydrophone sensors prevent us from separating a wavefield. One limitation on the practical application of seismic interferometry is the generation of crosstalk or artifacts by crosscorrelation (Guo et al., 2015). In most practical cases using a controlled source for regional-scale or crustal-scale surveys, the fundamental assumption of a boundary condition for seismic interferometry (Wapenaar and Fokkema, 2006) cannot be satisfied. For crustal-scale OBS surveys, wide source-receiver aperture data are acquired with dense air-gun shots just below the sea surface and receivers sparsely deployed on the seafloor along a survey line extending hundreds of kilometers. The sparseness of the receivers can cause not only crosstalk but also spatial aliasing artifacts.

Carriere and Gerstoft (2013) apply interferometric redatuming to common source gathers of the air gun-OBS data with 25 m OBS spacing. They image the shallow subsurface structures using redatumed data at OBS locations on the seafloor. For lithospheric-scale seismic structural surveys with more than 1 km OBS spacing, imaging detail subseafloor structures by redatuming at OBS locations is difficult. Jiang et al. (2005) present an example of interferometric imaging for multiple reflections of 3D vertical seismic profiling (VSP) data. The enlarged imaging result obtained using the multiple reflections is comparable with the result of a conventional reflection survey with a streamer cable system. In our study, we applied seismic interferometry to the common receiver gathers of an actual wide-angle OBS data set obtained in a plate subduction zone. We also applied seismic imaging to the redatumed data set. Then, we examined the dependence of imaging results on the data acquisition parameters and data processing parameters by application of various comparison tests for further practical applications of interferometric OBS imaging.

INTERFEROMETRIC OBS IMAGING

Actually, interferometric OBS imaging is based on two-part processing: redatuming multiple reflections using seismic interferometry and reflection imaging using redatumed data. Figure 1 portrays a concept of interferometric redatuming. We apply seismic interferometry to common receiver gathers of the air gun-OBS data. By correlating the seismic records obtained from different shots, the receiver-side multiple reflections are redatumed to the primary reflections. Sources and receivers of the redatumed data are located at all original air-gun shot positions. Generally, in the OBS survey, very long offset data are acquired with dense air-gun shots and sparse receivers. The imaging area by the original primary reflections is limited beneath each OBS (Figure 2a). Therefore, spatially continuous imaging is difficult between those OBSs. The imaging area with a single OBS is enlarged as a result of interferometric redatuming. The final reflection profile is obtainable continuously from just below the sea floor to the deeper regions of the crustal structure (Figure 2b).

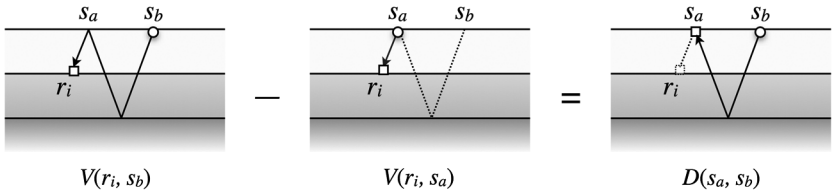

Figure 1. Basic concept of the interferometric redatuming of air gun-OBS data. Primary reflection data $D(s_a, s_b)$ are synthesized by the interference of seismic records $V(r_i, s_b)$ and $V(r_i, s_a)$ of OBS at r_i due to different shots at s_a and s_b.

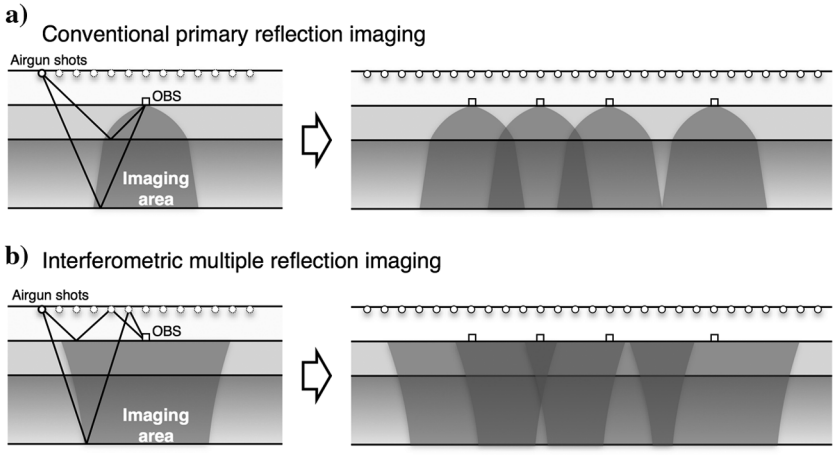

Figure 2. Schematic diagram of interferometric OBS imaging. (a) Conventional primary reflection imaging and (b) interferometric multiple reflection imaging from the air-gun-OBS data. As a result of the enlarged imaging area by interferometric redatuming, a continuous reflection image is obtainable along the whole shooting line.

We compared two interferometry techniques: deconvolution interferometry (Vasconcelos and Snieder, 2008a) and crosscorrelation interferometry (Wapenaar and Fokkema, 2006). Deconvolution interferometry is given by the following expression in a frequency domain:

$$D(s_a, s_b, \omega) = \sum_i^n \left[\frac{V(r_i, s_a, \omega)}{V(r_i, s_b, \omega)}\right], \quad (1)$$

where s_a and s_b denote the respective locations of different air-gun shots, r_i is a location of the ith OBS, n represents the total number of OBSs,

and ω is an angular frequency. The right side presents the summation after deconvolution of two seismic traces due to different shots, $V(r_i, s_a, \omega)$ and $V(r_i, s_b, \omega)$. The seismic trace $D(s_a, s_b, \omega)$ is a synthesized record at s_a due to a virtual source at s_b. If the seismic trace $V(r_i, s_a, \omega)$ is defined as a convolution of a source wavelet $W(s_a, \omega)$, a Green's function $G(r_i, s_a, \omega)$, and a receiver response $R(r_i, \omega)$, then equation 1 can be expressed as

$$D(s_a, s_b, \omega) = \sum_i^n \frac{W(s_a, \omega)G(r_i, s_a, \omega)R(r_i, \omega)}{W(s_b, \omega)G(r_i, s_b, \omega)R(r_i, \omega)}. \quad (2)$$

If the source wavelets can be regarded as the same in a survey using a controlled air gun source as $W(s_a, \omega) = W(s_b, \omega)$, then we can rewrite equation 2 as

$$D(s_a, s_b, \omega) = \sum_i^n \frac{G(r_i, s_a, \omega)}{G(r_i, s_b, \omega)}, \quad (3)$$

without the source wavelets and receiver responses.

In correlation interferometry, the seismic trace $C(s_a, s_b, \omega)$ is synthesized using the following equation in a frequency domain:

$$C(s_a, s_b, \omega) = \sum_i^n V(r_i, s_a, \omega)V^*(r_i, s_b, \omega). \quad (4)$$

The asterisk "$*$" denotes a complex conjugate. By substituting source wavelets and receiver responses, equation 4 can be rewritten as

$$C(s_a,s_b,\omega) = \sum_i^n W(s_a,\omega)G(r_i,s_a,\omega) \times R(r_i,\omega)W^*(s_b,\omega)G^*(r_i,s_b,\omega)R^*(r_i,\omega). \quad (5)$$

If $W(s_a, \omega) = W(s_b, \omega) = W(\omega)$, then

$$C(s_a,s_b,\omega) = |W(\omega)|^2 \sum_i^n |R(r_i,\omega)|^2 G(r_i,s_a,\omega)G^*(r_i,s_b,\omega). \quad (6)$$

In this equation, the effects of the source and receiver remain.

In comparing equation 3 with 6, the inherent effects of source and receiver can be canceled naturally using deconvolution interferometry. Consequently, we can expect image quality improvement if the source wavelet is not tuned as an ideal impulsive shape or if receivers of several kinds with different inherent responses are used for data acquisition.

In practice, the deconvolution operator can be unstable if the denominator is extremely small. To avoid this instability, we adopt stabilization by the water-level method (Clayton and Wiggins, 1976; Ammon, 1991; Vasconcelos and Snieder, 2008b) for calculating the deconvolution in equation 1 as

$$D(s_a,s_b,\omega) = \sum_i^n \left[\frac{V(r_i,s_a,\omega)V^*(r_i,s_b,\omega)}{\max\{|V(r_i,s_b,\omega)|^2, c\cdot|V(r_i,s_b,\omega)|^2_{\max}\}} \right], \quad (7)$$

where the asterisk $*$ denotes a complex conjugate, and constant c is a factor determining the minimum amplitude in the denominator. Also, $|V(r_i, s_b, \omega)|^2_{\max}$ is the maximum value of the power of $V(r_i, s_b, \omega)$ in the whole frequency range. If c is large, the denominator of equation 7 becomes a constant, and the deconvolution interferometry approximates the crosscorrelation interferometry (Vasconcelos and Snieder, 2008b). When it is too small, the deconvolution becomes unstable. We used a value of 0.01 for this study.

APPLICATION TO FIELD DATA

Survey area and data

We applied seismic interferometry to wide-angle OBS survey data acquired in a Nankai Trough subduction zone located southwest of Japan, where the Philippine Sea plate is subducting beneath the Eurasian plate with a splay fault system (Figure 3). Many seismic surveys using MCS and OBS have been conducted to elucidate characteristics of the seismogenic zone such as the shape and the characteristics of the subducted plate interface (Kodaira et al., 2000; Nakanishi et al., 2002, 2008; Park et al., 2002; Taira et al., 2005; Moore et al., 2009). After using high-resolution MCS surveys, Park et al. (2002) report the splay fault system characteristics. Moore et al. (2007) present detailed 3D geometry of the splay faults and the accretionary prism thrusts based on a 3D MCS survey. Wide-angle OBS surveys have revealed detailed velocity structures based

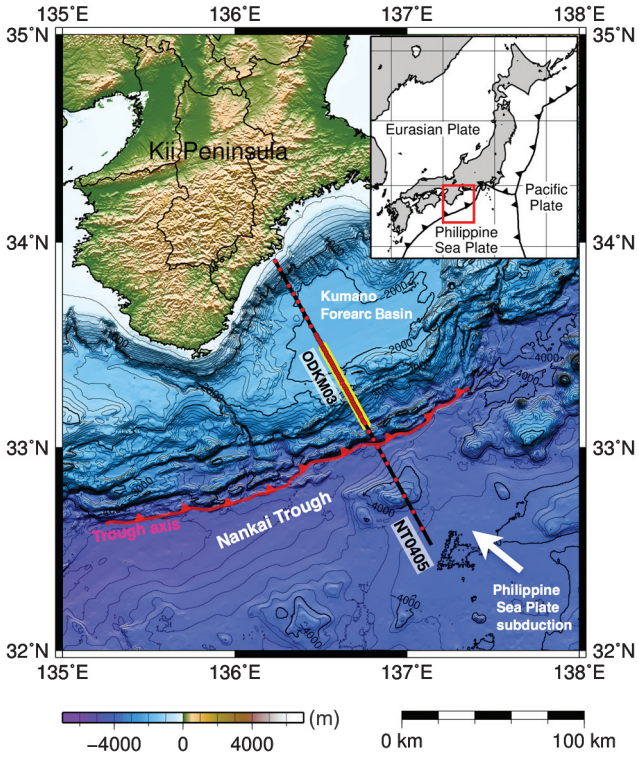

Figure 3. Map of the wide-angle OBS survey in Nankai Trough off the Kii Peninsula, southwestern Japan, in 2004 by JAMSTEC (NT0405). A thick black line shows the air-gun shot line. The red circles show the locations of the OBSs. The bold yellow line along the OBS survey line shows the previous 2D MCS survey line (ODKM03).

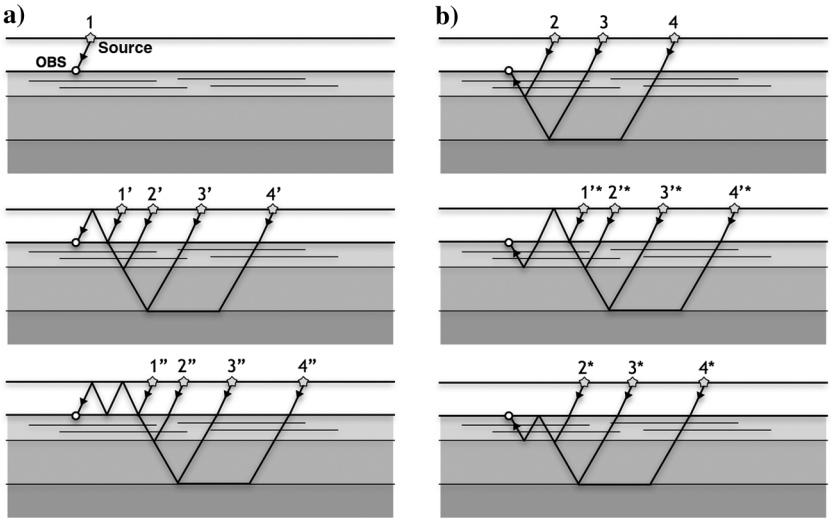

Figure 14. Schematics of raypaths in the air gun-OBS survey. (a) Down-going wave arrivals. (b) Up-going wave arrivals. Numbers with superscripts denote some possible raypaths. The single quotation mark (') and double quotation mark ("), respectively, denote the first-order and second-order multiples in a water layer. The asterisk (*) denotes a first-order reflection path in a shallow subsurface layer.

Towing long streamer cables is not practical in areas with heavy ship traffic. Consequently, many lithospheric-scale seismic structural surveys conducted by academic institutes often lack coincident MCS data sets. In such cases, interferometric OBS imaging can provide reflection images of shallow structures. In addition, the long-offset data sets with low-frequency energy of OBS surveys are expected to be more effective for imaging deeper structures than the limited offset data of MCS surveys.

CONCLUSION

We achieved continuous reflection imaging of complex structures in a subduction zone using interferometric OBS imaging. Seismic interferometry enables data-driven redatuming of surface-related multiple reflections for reflection imaging from wide-angle OBS data, even if only a single component is available. Results of enlarged illumination areas of the respective OBSs show that whole subsurface structures from the seafloor can be imaged. Deconvolution interferometry yields a better image than correlation interferometry does because the source and receiver responses can be removed automatically in application to the common receiver gathers and because reverberation artifacts in the correlation image can be suppressed by deconvolution interferometry. To improve the final image, parameter tests are necessary. The offset range and the record length are important parameters for application of interferometric redatuming. Air-gun-to-OBS distance of up to 50 km and input data record length of 80 s are necessary to suppress noise and to improve illumination in our case study. The most important parameter is the OBS spacing. For lithospheric-scale surveys in deep water of thousands of meters using low-frequency signals (<30 Hz), our results demonstrate that 10 km OBS spacing can image horizontal reflectors, and they demonstrate that 5 km OBS spacing can yield images of oblique interfaces such as the splay fault and top of the oceanic crust in the subduction zones. For further quantitative investigation, understanding crosstalk effects due to the acquisition setting will be useful to optimize methods for eliminating them before and after interferometric redatuming. Interferometric OBS imaging is an especially effective method to reanalyze old OBS data sets that have no coincident MCS data. We verified interferometric OBS imaging as a powerful method for deep subsurface structures by merging primary reflection imaging with interferometric multiple reflection imaging. By applying interferometric OBS imaging with other advanced analysis methods, full waveform information can be highly used for crustal structure imaging.

ACKNOWLEDGMENTS

We thank J. Etgen, J. van der Neut, and three anonymous reviewers for useful comments and suggestions.

REFERENCES

Ammon, C. J., 1991, The isolation of receiver effects from teleseismic P waveforms: Bulletin of the Seismological Society of America, **81**, 2504–2510.

Carriere, O., and P. Gerstoft, 2013, Deep-water subsurface imaging using OBS interferometry: Geophysics, **78**, no. 2, Q15–Q24, doi: 10.1190/geo2012-0241.1.

Clayton, R. W., and R. A. Wiggins, 1976, Source shape estimation and deconvolution of teleseismic bodywaves: Geophysical Journal of the Royal Astronomical Society, **47**, 151–177, doi: 10.1111/j.1365-246X.1976.tb01267.x.

Dash, R., G. Spence, R. Hyndman, S. Grion, Y. Wang, and S. Ronen, 2009, Wide-area imaging from OBS multiples: Geophysics, **74**, no. 6, Q41–Q47, doi: 10.1190/1.3223623.

Grion, S., R. Exley, M. Manin, X.-G. Miao, A. Pica, Y. Wang, P.-Y. Granger, and S. Ronen, 2007, Mirror imaging of OBS data: First Break, **25**, 37–42, doi: 10.3997/1365-2397.2007028.

Guo, B., J. Yu, Y. Huang, S. M. Hanafy, and G. T. Schuster, 2015, Benefits and limitations of imaging multiples: Interferometric and resonant migration: The Leading Edge, **34**, 802–805, doi: 10.1190/tle34070802.1.

Hanafy, S. M., Y. Huang, and G. T. Schuster, 2015, Benefits and limitations of imaging multiples: Mirror migration: The Leading Edge, **34**, 796–800, doi: 10.1190/tle34070796.1.

Jiang, Z., Z. Yu, G. T. Schuster, and B. E. Hornby, 2005, Migration of multiples: The Leading Edge, **24**, 315–318, doi: 10.1190/1.1895318.

Kamei, R., R. G. Pratt, and T. Tsuji, 2012, Waveform tomography imaging of a megasplay fault system in the seismogenic Nankai subduction zone: Earth and Planetary Science Letters, **317–318**, 343–353.

Kamei, R., R. G. Pratt, and T. Tsuji, 2013, On acoustic waveform tomography of wide-angle OBS data — Strategies for pre-conditioning and inversion: Geophysical Journal International, **194**, 1250–1280, doi: 10.1093/gji/ggt165.

Kodaira, S., N. Takahashi, A. Nakanishi, S. Miura, and Y. Kaneda, 2000, Subducted seamount imaged in the rupture zone of the 1946 Nankai earthquake: Science, **289**, 104–106, doi: 10.1126/science.289.5476.104.

Mehta, K., A. Bakulin, J. Sheiman, R. Calvert, and R. Snieder, 2007, Improving the virtual source method by wavefield separation: Geophysics, **72**, no. 4, V79–V86, doi: 10.1190/1.2733020.

Moore, G. F., N. L. Bangs, A. Taira, S. Kuramoto, E. Pangborn, and H. J. Tobin, 2007, Three-dimensional splay fault geometry and implications for tsunami generation: Science, **318**, 1128–1131, doi: 10.1126/science.1147195.

Moore, G. F., J.-O. Park, N. L. Bangs, S. P. Gulick, H. J. Tobin, Y. Nakamura, S. Sato, T. Tsuji, T. Yoro, H. Tanaka, S. Uraki, Y. Kido, Y. Sanada, S. Kuramoto, and A. Taira, 2009, Structural and seismic stratigraphic framework of the NanTroSEIZE Stage 1 transect: Proceedings of the Integrated Ocean Drilling Program, Volume **314**/315/316.

Nakanishi, A., S. Kodaira, S. Miura, A. Ito, T. Sato, J.-O. Park, Y. Kido, and Y. Kaneda, 2008, Detailed structural image around splay-fault branching in the Nankai subduction seismogenic zone: Results from a high-density ocean bottom seismic survey: Journal of Geophysical Research, **113**, B03105, doi: 10.1029/2007JB004974.

Nakanishi, A., N. Takahashi, J.-O. Park, S. Miura, S. Kodaira, Y. Kaneda, N. Hirata, T. Iwasaki, and M. Nakamura, 2002, Crustal structure across the coseismic rupture zone of the 1944 Tonankai earthquake, the central Nankai Trough seismogenic zone: Journal of Geophysical Research, **107**, EPM 2-1–EPM 2-21, doi: 10.1029/2001JB000424.

Park, J.-O., T. Tsuru, S. Kodaira, P. R. Cummins, and Y. Kaneda, 2002, Splay fault branching along the Nankai subduction zone: Science, **297**, 1157–1160, doi: 10.1126/science.1074111.

Ruigrok, E. N., D. S. Draganov, J. Thorbecke, J. R. van der Neut, and K. Wapenaar, 2008, Sampling and illumination aspects of seismic interferometry in horizontally layered media: 70th Annual International Conference and Exhibition, EAGE, Extended Abstracts, P277.

Schuster, G. T., 2009, Seismic interferometry: Cambridge University Press.

Taira, A., D. Curewitz, T. Hashimoto, A. Ibusuki, S. Kuramoto, T. Okano, and H. Tanaka, 2005, Nankai Trough seismogenic zone site survey: Kumano basin seismic survey, Philippine Sea, offshore Kii Peninsula, Japan: CDEX Technical Report, Volume 1.

Vasconcelos, I., and R. Snieder, 2008a, Interferometry by deconvolution, Part 1 — Theory for acoustic waves and numerical examples: Geophysics, **73**, no. 3, S115–S128, doi: 10.1190/1.2904554.

Vasconcelos, I., and R. Snieder, 2008b, Interferometry by deconvolution, Part 2 — Theory for elastic waves and application to drill-bit seismic imaging: Geophysics, **73**, no. 3, S129–S141, doi: 10.1190/1.2904985.

Wapenaar, K., D. Draganov, R. Snieder, X. Campman, and A. Verdel, 2010, Tutorial on seismic interferometry: Part 1 — Basic principles and applications: Geophysics, **75**, no. 5, 75A195–75A209, doi: 10.1190/1.3457445.

Wapenaar, K., and J. Fokkema, 2006, Green's function representation for seismic interferometry: Geophysics, **71**, no. 4, SI33–SI46, doi: 10.1190/1.2213955.